Arch. Metall. Mater. **65** (2020), 3, 1105-1110

DOI: 10.24425/amm.2020.133225

CHUL-HEE LEE[1], PEYALA DHARMAIAH[1], JUN-WOO SONG[1],
KWANG-YONG JEONG[1], SOON-JIK HONG[1*]

INFLUENCE OF SPARK PLASMA SINTERING TEMPERATURE ON MICROSTRUCTURE AND TTHERMOELECTRIC PROPERTIES OF Cu-DOPED $Bi_{0.5}Sb_{1.495}Te_3$ COMPOUND

Due to air pollution, global warming and energy shortage demands new clean energy conversion technologies. The conversion of industrial waste heat into useful electricity using thermoelectric (TE) technology is a promising method in recent decades. Still, its applications are limited by the low efficiency of TE materials in the operating range between 400-600 K. In this work, we have fabricated $Cu_{0.005}Bi_{0.5}Sb_{1.495}Te_3$ powder using a single step gas atomization process followed by spark plasma sintering at different temperatures (623, 673, 723, and 773 K), and their thermoelectric properties were investigated. The variation of sintering temperature showed a significant impact on the grain size. The Seebeck coefficient values at room temperature increased significantly from 127 μVK to 151 μV/K with increasing sintering temperature from 623 K to 723 K due to decreased carrier concentration. The maximum *ZT* values for the four samples were similar in the range between 1.15 to 1.18 at 450 K, which suggest these materials could be used for power generation in the mid-temperature range (400-600 K).

Keywords: Bismuth antimony telluride; gas atomization; spark plasma sintering; microstructure, thermoelectric materials

1. Introduction

Efforts to develop new sources for green energy harvesting have been continued with the increased risk of environmental pollution and energy depletion. Among them, thermoelectric materials are gaining much attention in recent days since they can convert waste heat into electricity and vice versa without greenhouse gas emissions [1,2]. Recently, Rattner et al. [3] reported that the estimated USA waste heat energy about 78% emitted from vehicles and power plant condensers and coolant was in low-temperature range (<200°C). It is well known that Bi-Sb-Te based materials exhibited high thermoelectric performance at room temperature. Thus, these materials can be utilized for power generation. The waste heat recovery efficiency of TE materials can be characterized by the dimensionless figure of merit *ZT*, expressed as $ZT = S^2\sigma T/\kappa$, where *S* is the Seebeck coefficient, σ is the electrical conductivity, κ is the total thermal conductivity consisting of electronic (κ_{el}), and lattice (κ_L) contributions and *T* is the operating temperature. The prevailing trend of recent research is mainly focused on elevating of ZT by tuning of dependent parameters (*S*, σ, κ) through modulation doping [4], band engineering [5], nano-inclusions [6] and hierarchical architecture designing [7].

Bismuth antimony tellurides are typically layered structure belonging to the rhombohedral crystal system and weakly bonded by van der Waals interaction [8-10]. Previous studies have shown that the absolute value of *S* drastically reduced by the excitation of minority carriers at elevated temperatures due to narrow bandgap (0.13-0.15 eV). For instance, Seo et al. [11] prepared $Bi_{0.5}Sb_{1.5}Te_3$ powders by combining attrition milling and SPS; attained the highest values of *S* and *ZT* at 75°C. Kim et al. [12] reported that the incorporation of Ta_2O_5 nanoparticles (NPs) into $Bi_{0.5}Sb_{1.5}Te_3$ matrix led to a remarkable enhancement of *S* (295 μV/K) and reduction of thermal conductivity at 300 K, exhibited a maximum *ZT* of 1.38 at 300 K. Yu et al. [13] obtained a peak *ZT* of 1.42 at 348 K for twin dominant microstructure by liquid state manipulation and spark plasma sintering. Most of the reported work on BiSbTe-based materials showed maximum thermoelectric performance in the range of 300-350 K, then after severely degraded due to enhanced κ and quickly declined *S*, so it is difficult to apply in mid-temperature range (400-600 K). To solve this limitation, researchers have been adopted alloying

[1] KONGJU NATIONAL UNIVERSITY, DIVISION OF ADVANCED MATERIALS ENGINEERING, 275, BUDAE-DONG, CHEONAN CITY, CHUNGCHEONGNAM-DO, 330-717, REPUBLIC OF KOREA

* Corresponding author: hongsj@kongju.ac.kr

or doping a tiny amount of Ag, Cu, Cd, Pb into BiSbTe system to improve the *ZT* to 1.0-1.4 at 453 K by lowering the lattice thermal conductivity via strengthening the phonon scattering and suppressing intrinsic excitation [5,14]. Among them, Cu is an effective dopant for suppression of bipolar contribution to increasing and widening of peak *ZT* values in BiSbTe materials. To obtain polycrystalline *p-type* Bi-Sb-Te materials with high thermoelectric performance and excellent mechanical strength for large-scale applications, various powder metallurgy techniques have been utilized, which includes ball milling and hot-pressing [15], gas-atomization and spark plasma sintering [2,6], and melt-spinning followed by spark plasma sintering [16].

In this study, $Cu_{0.005}Bi_{0.5}Sb_{1.495}Te_3$ powder was fabricated using a single step gas atomization process followed by spark plasma sintering at different temperatures (623, 673, 723, and 773 K). The grain texture and the thermoelectric properties of bulk samples were investigated. The grain size increased with increasing sintering temperature. All samples exhibited high *ZT* values above unity in the temperature range of 400 to 500 K, which suggest these materials could be used for power generation in the mid-temperature range (400-600 K).

2. Experimental procedure

The composition of $Cu_{0.005}Bi_{0.5}Sb_{1.495}Te_3$ powder was prepared by gas atomization process using high purity (>99.99%) elemental granules of Bi, Sb, Te and Cu (purchased from Alfa Aesar Co. Ltd). The granules were melted by high-frequency induction furnace in a graphite crucible at a temperature of above 400°C under argon atmosphere. The molten melt was atomized by pouring through boron nitride nozzle of 5-mm internal diameter into a confined N_2 gas at a pressure of 1.2 MPa [17,18]. Then, the conventional mechanical sieving method was used to obtain a powder size of about less than 200 μm. The gas atomized powder was consolidated into bulk material using spark plasma sintering (SPS) at various temperatures (623, 673, 723, and 773 K) for 10 min under an axial pressure of 50 MPa. The phase structure of the samples was characterized by X-ray diffraction (XRD) (MiniFlex-600/Rigaku/Japan) using high-energy monochromatic CuKα radiation (1.5418 Å) in the range of 10° to 60° with a step size of 0.02°. The powder morphologies and microstructure of bulks were observed using scanning electron microscopy (SEM-MIRA-LMH 2 (TESKAN)), and electron backscatter diffraction (EBSD/JEOL-7000F), respectively. The density (d) of bulk samples was measured several times by the Archimedes method, and these values were averaged for better accuracy. To measure the Seebeck coefficient and electrical conductivity, bulks were cut into bar shape with dimensions of $4 \times 4 \times 12$ mm^3 using a wire cutting machine. The total thermal conductivity (κ) was calculated using equation $\kappa = \lambda C_p d$, where λ is the thermal diffusivity measured using laser flash method (LFA-457 (Netzsch)), C_p is the specific heat measured by differential scanning calorimetry via Perkin Elmer DSC-8000 system, and d is the density. The carrier concentration (n_c) and mobility (μ_c) were measured using the Hall measurement system (HMS-3000 (Ecopia)) with the magnetic field of 0.55 T.

3. Results and discussion

The scanning electron microscopy (SEM) images of $Cu_{0.005}Bi_{0.5}Sb_{1.495}Te_3$ thermoelectric powders prepared by the gas atomization process are shown in Fig. 1. The gas atomized $Cu_{0.005}Bi_{0.5}Sb_{1.495}Te_3$ powder shows spherical morphology regardless of the particle size, and some of the particles had few small satellites on the surface. Also, the polygonal shape can be observed on the powder surface, which is considered to the hexagonal structure inherent of the BiSbTe based materials. The average particle size is estimated to be about 20 μm.

Fig. 2 show the X-ray diffraction patterns of the initial powder and bulk samples fabricated by spark plasma sintering

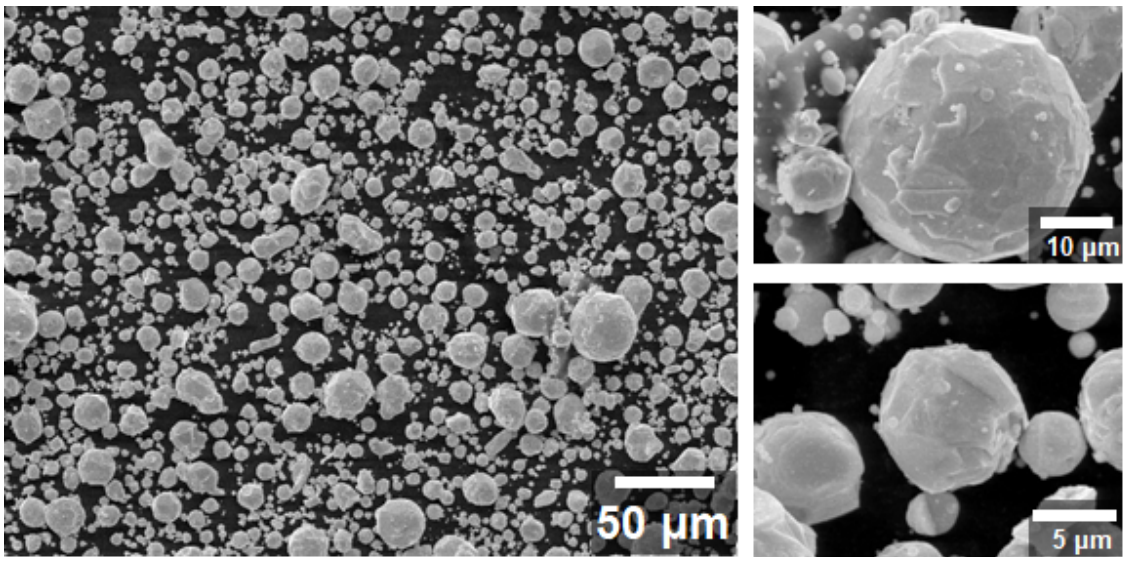

Fig. 1. SEM morphology of $Cu_{0.005}Bi_{0.5}Sb_{1.495}Te_3$ powder fabricated by gas atomization process

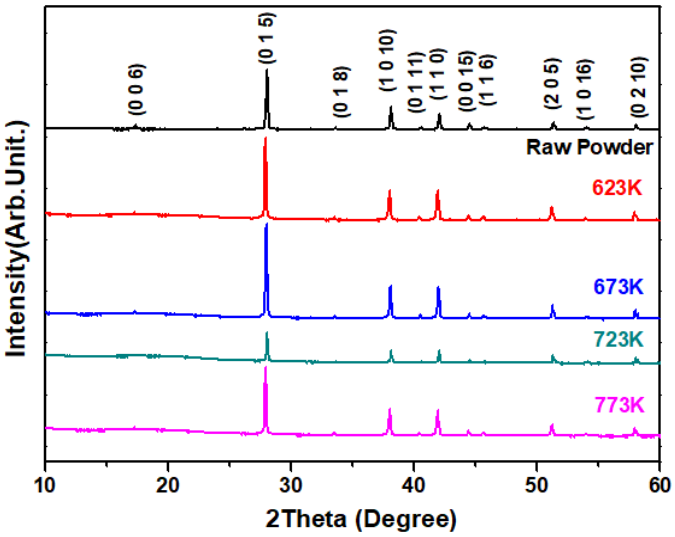

Fig. 2. X-ray diffraction pattern of $Cu_{0.005}Bi_{0.5}Sb_{1.495}Te_3$ powder fabricated by gas atomization and their bulk samples obtained by spark plasma sintering at different temperatures

at different temperatures. The XRD patterns of all samples were observed as a single phase with the rhombohedral structure of $Bi_{0.5}Sb_{1.5}Te_3$ (space group: $R\bar{3}m$; JCPDS#491713), and the impurity phase relative to Cu content was not detected. The relative density of all bulk samples was nearly close to each other and exhibited more than 99% of their theoretical density (see Table 1).

Fig. 3 shows the EBSD inverse pole figure maps of the bulk samples obtained at different sintering temperatures. It can be observed that the grain textures are randomly oriented and well-compacted grains, which agrees with density measurements. The grain size increased with increasing sintering temperature from 623 K to 773 K. The quantitative grain sizes of the bulk samples were estimated to be 9 μm, 12 μm, 17 μm and 19 μm for 623 K, 673 K, 723 K, and 773 K, respectively.

TABLE 1

The relative density, carrier concentration n_c, mobility μ_c, Seebeck coefficient S, electrical conductivity σ, density of states effective mass (m^*/m_0) at room temperature

Sample	Relative density (%)	n_c (10^{19}/cm^3)	μ_c (cm^2/Vs)	S (μV/K)	σ (/Ωcm)	m^*/m_0
623 K	99.42	4.78	247.75	126.79	2131.13	0.89
673 K	99.19	3.42	279.76	146.17	1837.58	0.87
723 K	99.52	3.11	313.8	150.46	1661.72	0.85
773 K	99.56	2.99	328.09	146.52	1820.48	0.80

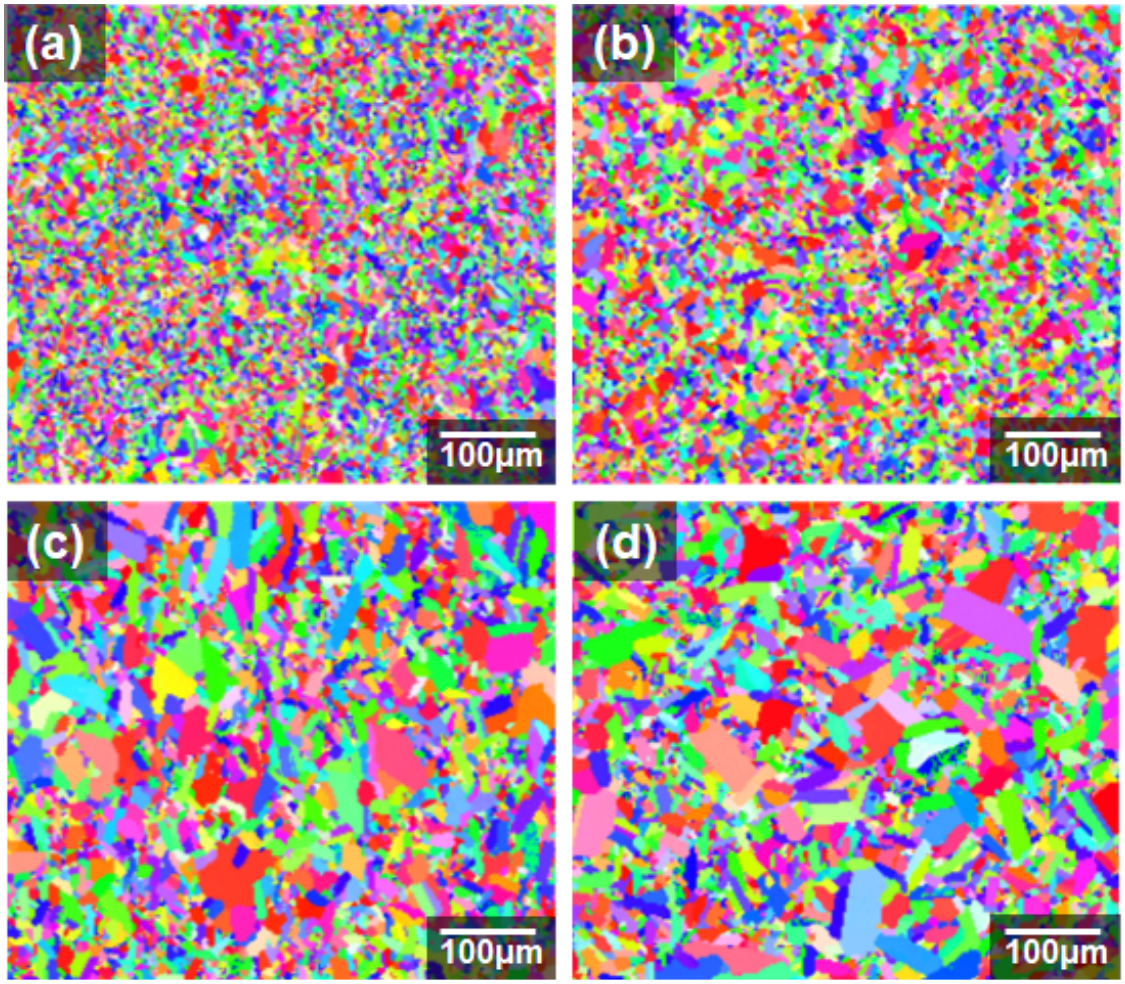

Fig. 3. Electron backscatter diffraction (EBSD) cross-sectional micrographs of the bulk samples obtained at different sintering temperatures: (a) 623 K, (b) 673 K, (c) 723 K, and (d) 773 K

The temperature dependence of the Seebeck coefficient (S), electrical conductivity (σ), and power factor for the $Cu_{0.005}Bi_{0.5}Sb_{1.495}Te_3$ samples obtained at different sintering temperatures are shown in Fig. 4. It can be seen from Fig. 4(a) that all the samples exhibited a positive sign of the Seebeck coefficient indicates holes are responsible for electronic transportation. The Seebeck coefficient for all the samples shows a similar tendency that they initially increase with increasing temperature, to reach a peak value at 475 K, and then decrease at elevated temperature due to intrinsic excitation of minority carriers [9]. The S values at room temperature increased significantly from 127 μVK to 151 μV/K with increasing sintering temperature from 623 K to 723 K and then slightly decreased with further increasing sintering temperature. The variation of S values with sintering temperature can be understood by the utilization of a single parabolic band model (SPB) [19]

$$S = \frac{k_B}{e}\left[\frac{\left(\frac{5}{2}+\lambda\right)F_{\frac{3}{2}+\lambda}(\xi_F)}{\left(\frac{3}{2}+\lambda\right)F_{\frac{1}{2}+\lambda}(\xi_F)} - \xi_F\right] \quad (1)$$

$$m^* = \frac{h^2}{2k_BT}\left(\frac{n_c}{4\pi F_{1/2}(\xi_F)}\right)^{\frac{2}{3}} \quad (2)$$

$$F_i(\xi_F) = \int_0^\infty \frac{x^i}{1+e^{x-\xi_F}}dx \quad (3)$$

$$\xi_F = \frac{E_f}{k_BT} \quad (4)$$

where E_f is the Fermi energy, ξ_F is the reduced Fermi level, $F_i(\xi_F)$ is the Fermi integral, k_B is the Boltzmann constant, h is the Planck's constant, λ is the scattering factor assuming as -0.5 for acoustic phonon scattering mode and e is the electronic charge. Thus, m^* values were estimated by using the experimental S and n_c at room temperature and listed in Table 1. The m^* values were nearly unchanged with increasing sintering temperature, which indicates that the band structure does not change. The enhanced Seebeck coefficient with sintering temperature is mainly due to the decreased n_c (Table 1).

The temperature dependence of electrical conductivity of $Cu_{0.005}Bi_{0.5}Sb_{1.495}Te_3$ samples obtained at different sintering temperatures is shown in Fig. 4(b). The electrical conductivity decreases monotonically with increasing measurement temperature, indicating a degenerate semiconducting behavior. In addition, the σ significantly reduced with increasing sintering temperature except for 773 K samples. As known, electrical conductivity depends on carrier concentration (n_c) and mobility (μ_c), which can be expressed as $\sigma = n_c e \mu_c$, where e is the electronic charge. Hall measurements indicate that the carrier concentration

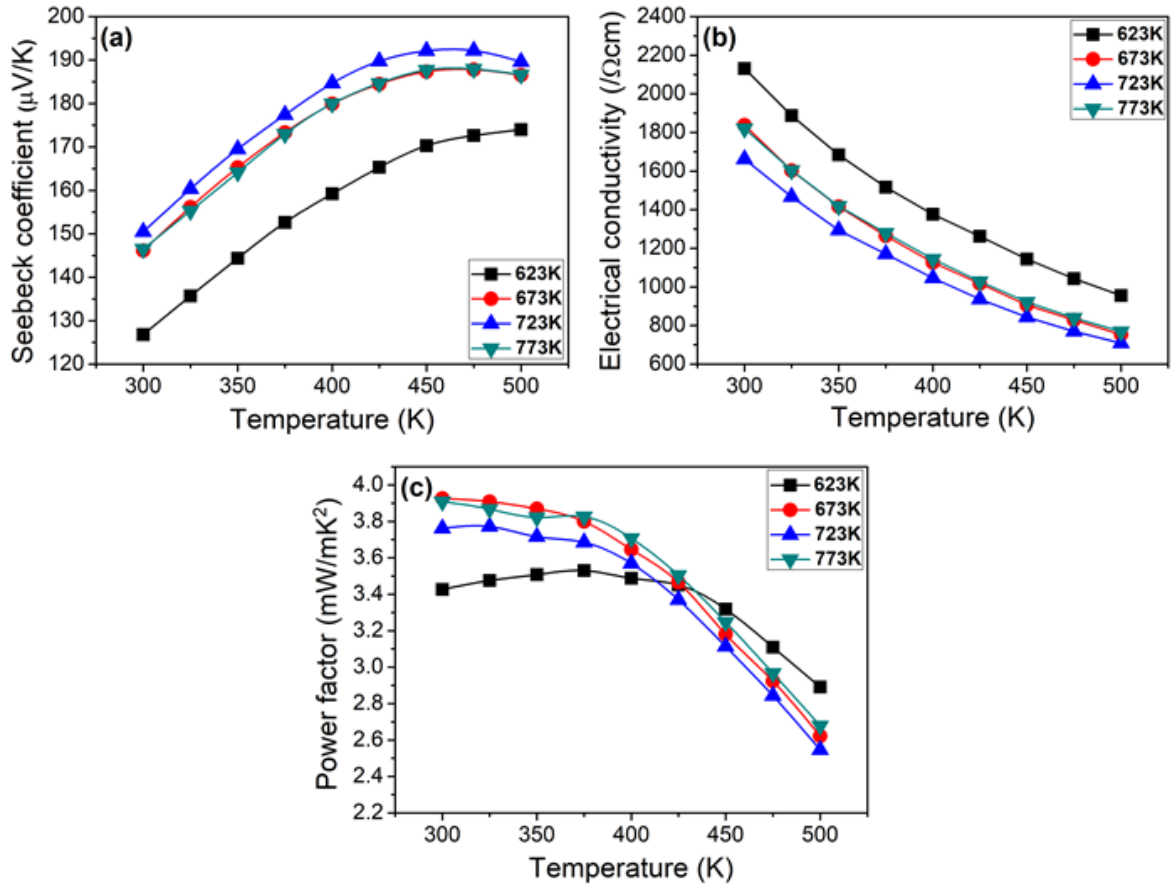

Fig. 4. Temperature dependence of electric transport properties of $Cu_{0.005}Bi_{0.5}Sb_{1.495}Te_3$ bulk samples with different sintering temperature: (a) Seebeck coefficient (S), (b) Electrical conductivity (σ), and (c) Power factor

decreased from 4.78 ×10^{19} cm^{-3} to 2.99 × 10^{19} cm^{-3}, while the carrier mobility significantly increased from 247.75 cm^2/Vs to 328.09 cm^2/Vs with increasing sintering temperature from 623 K to 773 K. According to the microstructure results, the grain size increased with increasing sintering temperature, which resulted in fewer grain boundaries, thus reducing the carrier scattering. This enables high mobility due to the easy carrier transport network [2]. Although carrier mobility increased with increasing sintering temperature, electrical conductivity decreased due to the decrease of carrier concentration.

Fig. 4(c) shows the temperature dependence of power factor (PF) for the samples obtained at different sintering temperatures. The PF values increased with increasing sintering temperature. It reached the highest value of 3.93 × 10^{-3} W/mK^2 at 300 K for the sample obtained at 673 K. The enhanced PF is attributed to increased Seebeck coefficient and less diminution of electrical conductivity.

Temperature dependence of total thermal conductivity (κ), electronic thermal conductivity (κ_{el}), and lattice thermal conductivity (κ_L) for the samples obtained at different sintering temperatures are shown in Fig. 5. The total thermal conductivity decreased gradually with temperature and then increased (above 450 K) with further increasing temperature. The room temperature thermal conductivity decreased from 1.60 W/mK to 1.49 W/mK as the sintering temperature increased from 623 K to 673 K. After that, the thermal conductivity again increased with increasing sintering temperature. However, the minimum thermal conductivity (1.26 W/mK) for all the samples quite close to each other at 450 K. It should be noticed that the minimum κ achieved at higher temperatures compared to the undoped $Bi_{0.5}Sb_{1.5}Te_3$ materials [2,13], due to suppression of bipolar thermal conduction by the increased concentration. Further, the total thermal conductivity is composed of electronic thermal conductivity (κ_{el}), and lattice thermal conductivity (κ_L). The κ_{el} can be estimated by the Wiedemann-Franz law, according to equation $\kappa_{el} = L\sigma T$, where L is Lorenz number, T is the absolute temperature. The values of L were calculated using S according to the following expression reported by Kim et al. [20]

$$L = 1.5 + \exp\left[-\frac{|S|}{116}\right] \quad (5)$$

It can be seen from Fig. 5(b) that as the sintering temperature increased, κ_{el} decreased, which is consistent with the electrical conductivity. The lattice thermal conductivity was obtained by subtraction of κ_{el} from κ and shown in Fig. 5(c). The κ_L values increased with increasing sintering temperature.

The temperature dependence of the figure of merit (ZT) for the samples obtained at different sintering temperatures was shown in Fig. 6. The room temperature ZT increased from 0.64 to 0.79 as the sintering temperature increased from 623 K to 673 K. However, the maximum ZT values for the four samples

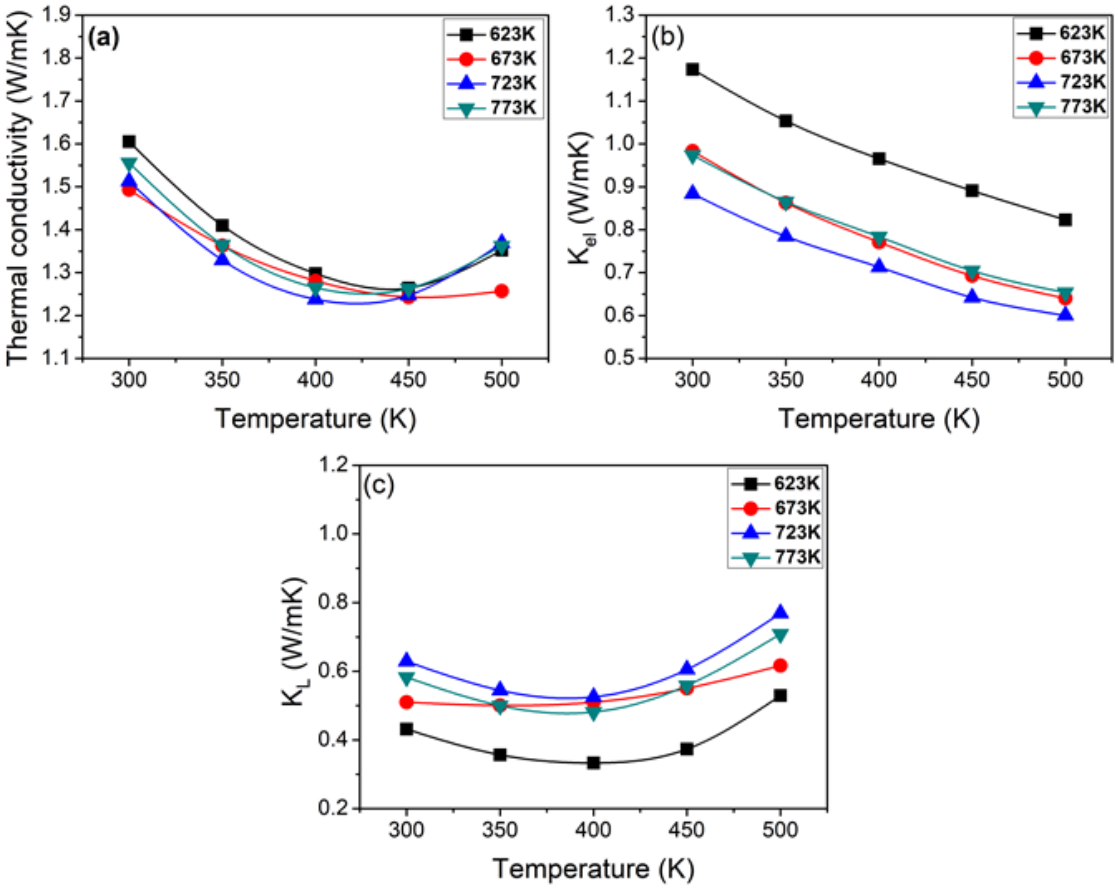

Fig. 5. Temperature dependence of thermal transport properties of $Cu_{0.005}Bi_{0.5}Sb_{1.495}Te_3$ bulk samples with different sintering temperature: (a) Total thermal conductivity (κ), (b) Electronic thermal conductivity (κ_{el}), and (c) Lattice thermal conductivity (κ_L)

were similar at 450 K in the range between 1.15 to 1.18. Overall, the four samples exhibited high *ZT* values above unity in the temperature range of 400 to 500 K, which suggest these materials can be used for power generation in the mid-temperature range (400-600 K).

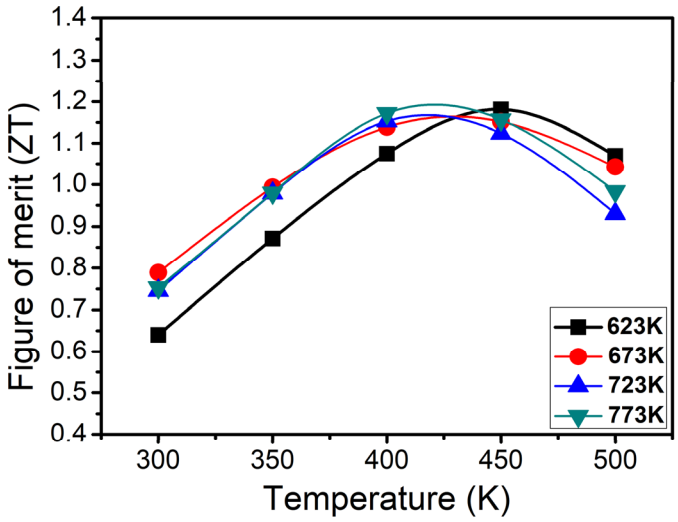

Fig. 6. Temperature dependence of figure of merit *ZT* for the samples obtained at different sintering temperatures

4. Conclusions

In this work, we have fabricated $Cu_{0.005}Bi_{0.5}Sb_{1.495}Te_3$ powder using a single step gas atomization process followed by spark plasma sintering at different temperatures (623, 673, 723, and 773 K), and their microstructure and thermoelectric properties were investigated. The variation of sintering temperature showed a significant impact on the grain size. The grain textures are randomly oriented and well-compacted grains, and their size increased with increasing sintering temperature. The results indicate that the Seebeck coefficient increased with increasing sintering temperature from 623 K to 723 K, while the electrical conductivity decreased due to the variation in carrier concentration and mobility. The thermal conductivity has also been decreased with increasing sintering temperature due to a decrease in electrical conductivity. The maximum *ZT* values for the four samples were similar in the range between 1.15 to 1.18 at 450 K, which suggest these materials could be used for power generation in the mid-temperature range (400-600 K).

Acknowledgments

This work was supported by the Basic Research Laboratory Program through the Ministry of Education of the Republic of Korea (2019R1A4A1026125).

This work was supported by the National Research Council ofScience & Technology (NST) grant by the Korea government (MSIP) (No. CRC-15-06-KIGAM).

REFERENCES

[1] J. He, T.M. Tritt, Science **357**, eaak9997 (2017).
[2] P. Dharmaiah, H.S. Kim, C.H. Lee, S.J. Hong, J. Alloys Compd. **686**, 1 (2016).
[3] A.S. Rattner, S. Garimella, Energy **36**, 6172-6183 (2011).
[4] M. Zebarjadi, G. Joshi, G. Zhu, B. Yu, A. Minnich, Y. Lan, X. Wang, M. Dresselhaus, Z. Ren, G. Chen, Nano Lett. **11**, 2225-2230 (2011).
[5] K. Kim, G. Kim, H. Lee, K.H. Lee, W. Lee, Scr. Mater. **145**, 41-44 (2018).
[6] E.B. Kim, P. Dharmaiah, K.H. Lee, C.H. Lee, J.H. Lee, J.K. Yang, D.H. Jang, D.S. Kim, S.J. Hong, J. Alloys Compd. **777**, 703-711 (2019).
[7] K. Biswas, J. He, I.D. Blum, C.I. Wu, T.P. Hogan, D.N. Seidman, V.P. Dravid, M.G. Kanatzidis, Nature **489**, 414-418 (2012).
[8] T. Fang, X. Li, C.L. Hu, Q. Zhang, J. Yang, W.Q. Zhang, X.B. Zhao, D.J. Sing, T.J. Zhu, Adv. Funct. Mater. **29**, 1900677 (2019).
[9] O.E. Femi, K. Akkiraju, B.S. Murthy, N. Ravisankar, K. Chattopadhyay, J. Alloys Compd. **682**, 791-798 (2016).
[10] K.H. Lee, P. Dharmaiah, S.J. Hong, Scr. Mater. **162**, 437-441 (2019).
[11] S. Seo, M.W. Oh, Y. Jeong, B. Yoo, J. Alloys Compd. **696**, 1151-1158 (2017).
[12] E.B. Kim, P. Dharmaiah, D. Shin, K.H. Lee, S.J. Hong, J. Alloys Compd. **703**, 614-623 (2017).
[13] Y. Yu, D.S. He, S. Zhang, O.C. Miredin, T. Schwarz, A. Stoffers, X.Y. Wang, S. Zheng, B. Zhu, C. Scheu, D. Wu, J.Q. He, M. Wuttig, Z.Y. Huang, F.Q. Zu, Nano Energy **37**, 203-213 (2017).
[14] F. Hao, P. Qiu, Y. Tang, S. Bai, T. Xing, H.S. Chu, Q. Zhang, P. Lu, T. Zhang, D. Ren, J. Chen, X. Shi, L. Chen, Energy Environ. Sci. **9**, 3120 (2016).
[15] B. Poudel, Q. Hao, Y. Ma, A. Minnich, B. Yu, X. Yan, D. Wang, A. Muto, D. Vashaee, X. Chen, J. Liu, M.S. Dresselhaus, G. Chen, Z. Ren, Science **320**, 634-638 (2008).
[16] W. Xie, J. He, H.J. Kang, X. Tang, S. Zhu, M. Laver, S. Wang, J.R. Copley, C.M. Brown, Q. Zhang, T.M. Tritt, Nano Lett. **10**, 3283-3289 (2010).
[17] S.M. Yoon, P. Dharmaiah, O.E. Femi, C.H. Lee, S.J. Hong, Mater. Chem. Phys. **195**, 49-57 (2017).
[18] S.J. Hong, B.S. Chun, Mater. Res. Bull. **38**, 599-608 (2003).
[19] Y. Pei, A.F. May, G.J. Snyder, Adv. Energy Mater. **1**, 291-296 (2011).
[20] H.S. Kim, Z.M. Gibbs, Y. Tang, H. Wang, G.J. Snyder, APL Mater. **3**, 041506 (2015).